Title
Monte Carlo Study of Domain Formation in YBa{sub 2}(Cu{sub 1-x}Fe{sub x}O{sub z}

Authors
Burmester, C.P.
Wille, L.T.
Gronsky, R.

Publication Date
1990-09-01

LBL-29593

Lawrence Berkeley Laboratory
UNIVERSITY OF CALIFORNIA

Materials & Chemical Sciences Division

Submitted to Solid State Communications

Monte Carlo Study of Domain Formation in $YBa_2(Cu_{1-x}Fe_x)_3O_z$

C.P. Burmester, L.T. Wille, and R. Gronsky

September 1990

Prepared for the U.S. Department of Energy under Contract Number DE-AC03-76SF00098

DISCLAIMER

LBL-29593

MONTE CARLO STUDY OF DOMAIN FORMATION IN $YBa_2(Cu_{1-x}Fe_x)_3O_z$

C.P. Burmester[1], L.T. Wille[2], and R. Gronsky[1]

[1]Dept. of Materials Science & Mineral Engineering
University of California, Berkeley
and
Materials and Chemical Sciences Division
National Center for Electron Microscopy
Lawrence Berkeley Laboratory
Berkeley, CA. 94720

[2]Department of Physics
Florida Atlantic University
Boca Raton, FL. 33431

This work was supported by the Director, Office of Energy Research, Office of Basic Energy Sciences, Material Sciences Division of the U.S. Department of Energy under Contract No. DE-AC03-76SF00098, and by grant No. MDA972-88-J-1006 from DARPA. Large scale numerical simulation was supported by a gift from Cray Research, Inc.

MONTE CARLO STUDY OF DOMAIN FORMATION IN $YBa_2(Cu_{1-x}Fe_x)_3O_z$

C. P. Burmester[1], L. T. Wille[2], and R. Gronsky[1]
[1]Department of Materials Science and Mineral Engineering, University of California, and Materials and Chemical Sciences Division, Lawrence Berkeley Laboratory, Berkeley, CA 94720, USA
[2]Department of Physics, Florida Atlantic University, Boca Raton, FL 33431, USA.

(Received 23 August 1990 by S. Amelinckx)

Upon progressive doping with Fe the $YBa_2(Cu_{1-x}Fe_x)_3O_z$ compound transforms from an orthorhombic to a tetragonal structure without an accompanying loss of superconductivity. This behavior has been interpreted by assuming that the tetragonal structure consists of many conflicting orthorhombic microdomains pinned by the Fe-atoms. Extending an Ising model previously used to model the undoped compound, we show by Monte Carlo simulation that such microdomains do indeed occur. The oxygen content is allowed to vary in the simulations, while the Fe-Cu sublattice is handled in the canonical ensemble (fixed Fe-content). The Fe-atoms are mobile and found to cluster along the <11> direction in precise agreement with experimental observations.

In order to understand the nature of the Cu-bonding in the $YBa_2Cu_3O_z$ superconducting compound and also with the aim of finding materials with improved superconducting properties, replacement of Cu by a variety of transition metal elements has been attempted.[1] It has been found experimentally that progressive substitution on the Cu(2) site (i.e. in the CuO_2 planes) leads to a very rapid decrease of the superconducting transition temperature T_c, while doping on the Cu(1) site (i.e. in the CuO basal plane) has a more moderate effect. This is in agreement with the recent understanding that the CuO basal plane, provided it is sufficiently ordered, acts mainly as a charge reservoir,[2] while the CuO_2 plane is the essential one as far as superconductivity in $YBa_2Cu_3O_z$ and the other superconducting cuprates is concerned. However, it is by now well established that the degree of oxygen order in the basal plane is equally important. If the oxygen atoms are randomly distributed the material possesses tetragonal symmetry and is non-superconducting, while ordered oxygen arrangements containing O-Cu-O chains lead to superconducting structures with orthorhombic symmetry.[3] Thus tetragonal symmetry in this class of materials came to be associated with the loss of superconductivity and it was therefore rather surprising when diffraction experiments[4-8] showed that upon increased doping of $YBa_2Cu_3O_z$ with certain elements (in particular, Fe, Co, Ga and Al) a transformation to the tetragonal structure occurs without any abrupt change in T_c. This puzzle was subsequently resolved[9-10] when it was found by high resolution electron microscopy that the tetragonal structure determined by X-ray or neutron diffraction actually possesses a high degree of local orthorhombic order and consists of many conflicting

microdomains pinned by the dopants, with O-Cu-O chains running in orthogonal directions within adjacent domains. Moreover, it was also concluded that the substituting atoms had a tendency to cluster along the <11> direction in the basal plane. It has been argued[10] that these effects can be understood in terms of the increased valence of these dopant elements (nominally 3+ or 4+, compared to Cu^{2+}), which leads to pseudo-tetrahedral four-fold or higher oxygen coordination. X-ray absorption[11] and Mossbauer[12] studies have shown that there are large distortions associated with those various configurations, while the latter work also indicates that the pseudo-tetrahedral arrangement is by far the most common one in Fe-doped material. Since the defects thus produced may act as flux pinning centers or weak links, a detailed understanding of the kinetics and equilibrium processes involved is of direct practical value. In the present work Monte Carlo simulations of a two-dimensional Ising model are used to elucidate the effects of doping on microstructure. To be specific, the discussion is cast in terms of Fe-doping but the arguments are expected to remain qualitatively valid for any trivalent dopant, such as Co, Ga, and Al.

To investigate the influence of dopant valence and coordination on local oxygen ordering, macroscopic symmetry, and dopant clustering behavior, a Monte Carlo simulation is developed which allows for the variation of dopant location and oxygen affinity. Extending previous work for the undoped case (reviewed in Ref. 3), the simulation lattice consists of two interpenetrating sublattices, an oxygen-vacancy lattice and a Cu-dopant lattice. Both lattices are treated separately in the calculation but are coupled in that the presence of a metal cation determines the magnitude and sign of the nearest and next nearest neighbor oxygen interactions in the dopant's "region of influence" defined for this model as depicted in Figure 1. No explicit Cu-Fe sublattice interactions are considered in the simulation and canonical exchanges between these two species are determined purely from the change in the configurational energy of the affected oxygens. The Cu(1) atom has been shown by many studies to prefer a square four-fold oxygen coordination which acts to order the Cu(1)-O(1) atoms into <010> chains in the basal plane leading to an overall orthorhombic structure. Basal plane cation dopants, however, can exist in various oxidation states leading to four-, five-, and six-fold coordinations with oxygen. While the simulation model is applicable to any basal plane dopant, it is possible to represent a specific dopant atom by considering the equilibrium bonding configurations for a particular choice of dopant. In the current case, the applicable cluster includes the cation and its four nearest oxygen-vacancy sublattice sites. The cluster interactions thus include four V_1 oxygen-vacancy sublattice interactions and the two V_2 oxygen-vacancy interactions bridged by the cation (see Figure 1). The relevant Hamiltonian for the oxygen-vacancy sublattice is thus

$$H^{O,V} = \sum^{nn} J(Cu,Fe)_1\sigma_i\sigma_j + \sum^{nnn'} J(Cu,Fe)_2\sigma_i\sigma_j + \sum^{nnn''} V_3\sigma_i\sigma_j - \sum^{n} \mu_O\sigma_i + \sum^{nn,\ cation} \mu(Cu,Fe)\sigma_i \quad (1)$$

where μ_O is the oxygen chemical potential, σ is the "pseudo-spin variable" specifying oxygen site occupancy (+1 denoting an occupied site, -1 a vacant site), μ(Cu,Fe), equal to μ_{Cu} or μ_{Fe}, is the cation influenced oxygen site potential, and $J(Cu,Fe)_i$ (i = 1,2) is either V_i or V_i', respectively, dependent on which cation influences the pair interaction while V_3, not influenced by a local cation environment, remains constant. By considering the dopant specific hierarchy of cluster energies, a set of bounding equations for the magnitudes and signs of the V_1 and V_2 pair interactions about the dopant site can be derived. In this manner, it has been shown that the oxygen ordering behavior in the CuO basal plane of $YBa_2Cu_3O_z$ is well modeled by an anisotropic next nearest neighbor Ising model with interaction parameters stabilizing the Cu-O chaining in the basal plane.[13-14] Iron is most commonly found to exist with a pseudo-tetrahedral coordination.[12] Within the basal plane, this is represented by a near 90° two-fold coordination of the iron with oxygen (see Figure 2). Iron can also assume five-fold pyramidal and six-fold octahedral coordinations which project to three- and four-fold basal plane oxygen coordinations. It is also known that the linear basal plane two-fold coordination commonly exhibited by the Cu(1) atom is an energetically unstable configuration for the iron atom. These two-, three-, and four-fold basal plane configurations for iron are schematically represented in Figure 2 along with their corresponding cluster energy configurations, E_1, E_2, E_3, and E_4. To derive the equations specifying the range of the V_1 and V_2 interactions for the case of iron in this model, the following conditions, based on the above discussed experimentally observed bonding configurations, are imposed: E_1 (square planar) > E_2 (octahedral) > E_3 (pyramidal) > E_4 (pseudo-tetrahedral). This establishes the following limitations on the choice of pair interactions for iron:

$$V_1' < 0 \quad (2)$$

and

$$V_2' > -2V_1'. \quad (3)$$

For the current set of simulations, the oxygen-vacancy interactions about an iron site are taken to be $V_1' = -1.0$ and $V_2' = 2.5$. Those about a copper site are taken to be $V_1 = 1.0$ and $V_2 = -0.5$. As the V_3 interaction is not site dependent in this model, it is taken to be $V_3 = 0.5$, as in the undoped case.[14] It is important to note that the pair interactions considered here

contain both electronic and elastic components. Some work has been performed in deriving the interactions for trivalent dopants from bonding considerations.[15-16] However, for the sake of comparison with results obtained in the undoped case,[14] the present choice of interactions has been adopted. It is expected that the qualitative behavior will remain the same for any choice of interaction parameters chosen within the limitations imposed by equations (2) and (3). Exchanges on the Cu-Fe sublattice are governed by the following Hamiltonian:

$$H^{Cu,Fe} = \left(\sum^{Cu,\ nn} V_1' \sigma_i \sigma_j + \sum^{Cu,\ nnn'} V_2' \sigma_i \sigma_j - \sum^{Cu,\ nn} \mu_{Fe} \sigma_j \right) - \left(\sum^{Fe,\ nn} V_1 \sigma_i \sigma_j + \sum^{Fe,\ nnn'} V_2 \sigma_i \sigma_j - \sum^{Fe,\ nn} \mu_{Cu} \sigma_j \right) \quad (4)$$

In the present work, the site potentials for iron and copper (μ_{Fe} and μ_{Cu}) have been taken to be equal, and the oxygen chemical potential, μ_O, has been held constant. As the oxygen chemical potential, μ_O, is related to oxygen partial pressure by:

$$\mu_O = \mu^o + \ln p_{O_2} \quad (5)$$

where μ^o is the reference chemical potential, this mimics experimental conditions. Monte Carlo simulations of Cu(1) doping have already been performed by other authors,[17-18] but previous studies do not allow for dopant mobility without which the clustering and kinetic behavior specifically associated with dopant driven transformations in the $YBa_2(Cu_xFe_{1-x})_3O_z$ system are not realistically modeled.

Monte Carlo simulation "snapshots" reveal that below the temperature corresponding to the orthorhombic to tetragonal transition in the simulations of the undoped compound,[14] the iron sites in the doped material form well defined <11> linear chains (Figure 3). The iron atoms in these diagonal chains exist with the two-fold, basal plane, pseudo-tetrahedral coordinations, as would be expected at an oxygen concentration near z = 7.0. It is found that the Fe-O clusters order in such a way that the resulting chains form twin boundaries separating orthogonal domain variants of the undoped orthorhombic basal plane Cu-O structure. By ordering in this fashion, the tetrahedrally coordinated iron sites can co-exist with the linear Cu-O structures while maintaining their preferred oxygen coordination. This leads to <11> iron chains in which the sites are not directly coupled by an oxygen bond. Instead, the stacking arises to satisfy purely configurational purposes leading to linear iron clustering extending far beyond an ordering wavelength that could be expected from nearest and next nearest neighbor interactions

alone. This basis for clustering has significant implications on the independent mobility of iron sites in the simulation. Since these sites are not directly bound by intervening oxygen atoms, an iron atom can move into a more favorable position based purely on oxygen coordination regardless of the nature of adjacent cation sites. It can also be argued that this kind of diagonal chaining minimizes the elastic strain associated with the presence of the tetrahedral FeO cluster in the predominantly linearly coordinated CuO basal plane. It is to be noted that while a large fraction of the Fe atoms participate in the diagonal clustering, isolated Fe atoms and atom clusters, which would act as strain centers, are frequently observed in the simulations (see Figure 3) in very good agreement with experiment.

The way in which Fe forms and populates domain boundaries in the simulation is seen to lead to macroscopic orthorhombic to tetragonal transitions as a function of Fe content alone. At low iron contents, the iron atoms form small isolated islands in a predominantly single domain orthorhombic structure (Figure 4). These islands have little effect on the overall symmetry and the structure reflects the local oxygen-vacancy sublattice crystallography. However, at higher iron contents, the iron atoms form the well ordered <11> linear clusters discussed above and, by percolating through the entire lattice, subdivide the basal plane into twinned orthorhombic regions of approximately equal variant proportion altering the macroscopic symmetry to be tetragonal even while the local symmetry on the oxygen-vacancy sublattice remains orthorhombic (Figure 3). This trend is represented schematically by plotting the percentage of oxygen sites lying in chains running in the [100] and [010] directions in the basal plane as a function of iron doping as is depicted in Figure 5. The orthorhombic to tetragonal transition occurs when the number of sites lying in either [100] or [010] orthorhombic domains becomes statistically equal. From the inflection point in Figure 5 this may be estimated to occur in this simulation at approximately 8.5 percent iron content in the basal plane ($x \cong 0.028$). While this is a rough estimate which has not been corrected for kinetic and finite size effects, it is well within the range of values that various authors have obtained for this transition.[19-20]

For the present simulations the number of attempted Monte Carlo moves per Fe atom is equal to that attempted per oxygen site. However, the kinetics associated with moves on the Cu-Fe sublattice is restricted by operating in the canonical scheme which only allows nearest neighbor exchanges. Moves on the oxygen-vacancy sublattice are calculated in the grand canonical scheme where the appearance of oxygen is influenced primarily by its chemical potential, unrestricted by exchange kinetics, and hence enjoy a larger degree of freedom. The effective mobility of Fe atoms for the current simulation model can thus be taken to be less than that of oxygen atoms. While it is plausible to assume that Fe atoms are less mobile than

oxygen atoms, the precise values are unknown at this stage and more experimental work will be needed to clarify this point. Clearly, dopant mobility will depend on both temperature and oxygen concentration (or partial pressure). It is known from tracer diffusion experiments[21] that the mobility of ^{57}Co in $YBa_2(Cu_{1-x}Co_x)_3O_z$ is much smaller than that of oxygen. Simulations are currently in progress to address these questions and will be reported at a later date. Preliminary results seem to indicate that for the given choice of interaction parameters, the clustering tendency of the dopant atoms is very strong and that diagonal <11> chains are rapidly attained, even for relatively small dopant mobilities.

While the present choice of interactions leads to results that are in remarkable agreement with experiment, it may be desirable to alter the energy equations such that four-, five-, and/or six-fold coordinations all become energetically favorable ($E < 0$) while retaining their energy hierarchy with respect to each other. This is impossible by considering the defined V_1 and V_2 interactions alone. However, by assigning a non-zero value to the iron site potential included in the Hamiltonian for this system, this can be achieved. Using the new conditions specified above as an example and recasting equations (2) and (3) to include this site potential, the new restrictions

$$\mu_{Fe} < 0 \tag{6}$$

and

$$\mu_{Fe} > -(2V_1' + V_2'). \tag{7}$$

are obtained. The inclusion of the cation site potential can also be used to re-order the cluster energy hierarchy. This capability becomes particularly useful when applying this model to the investigation of trivalent dopants other than iron. Monte Carlo simulations for parameters satisfying equations (6) and (7), and inequalities derived to model the behavior of other trivalent basal-plane dopants in the $YBa_2Cu_3O_z$ system are currently in progress and will be reported elsewhere.

Acknowledgements - The work at Berkeley is supported by the Director, Office of Basic Energy Sciences, Materials Sciences Division of the U. S. Department of Energy under Contract Number DE-AC03-76SF00098. One of us (L.T.W.) is supported by grant No. MDA 972-88-J-1006 from DARPA. Large scale numerical simulation was supported by a gift from Cray Research, Inc. L.T.W. acknowledges stimulating conversations with E. Liarokapis, Th. Leventouri, F. D. Medina, H. Oesterreicher, and L. T. Romano.

REFERENCES

1. R. Beyers and T. M. Shaw, *Sol. St. Phys.* **42**, 135 (1989).
2. Y. Tokura, J. B. Torrance, T. C. Huang, and A. I. Nazzal, *Phys. Rev.* **B38**, 7156 (1988).
3. L. T. Wille, *Phase Transitions* **22**, 225 (1990).
4. G. Xiao, M. Z. Cieplak, A. Gavrin, F. H. Streitz, A. Bakhshai, and C. L. Chien, *Phys. Rev. Lett.* **60**, 1446 (1988).
5. Y. Maeno, T. Tomita, M. Kayogoku, S. Awaji, Y. Aoki, K. Hoshino, A. Minami, and T. Fujita, *Nature* **328**, 512 (1987).
6. E. Tayakami-Muromachi, Y. Uchida, and K. Kato, *Jpn. J. Appl. Phys.* **26**, L2087, (1987).
7. T. J. Kistenmacher, W. A. Bryden, J. S. Morgan, K. Moorjani, Y. W. Du, Z. Q. Qiu, H. Tang, and J. C. Walker, *Phys. Rev.* **B36**, 8877 (1987).
8. J. M. Tarascon, P. Barboux, P. F. Miceli, L. H. Greene, G. W. Hull, M. Eibschutz, and S. A. Sunshine, *Phys. Rev.* **B37**, 7458 (1988).
9. G. Roth, G. Heger, B. Renker, J. Pannetier, V. Caignaert, M. Hervieu, and B. Raveau, *Z. Phys.* **B71**, 43 (1988).
10. P. Bordet, J. L. Hodeau, P. Strobel, M. Marezio, and A. Santoro, *Solid State Comm.* **66**, 435 (1988).
11. F. Bridges, J. B. Boyce, T. Cleason, T. H. Geballe, and J. M. Tarascon, *Phys. Rev.* **B39**, 11603 (1989).
12. B. D. Dunlap, J. D. Jorgensen, C. Segre, A. E. Dwight, J. L. Matykiewicz, H. Lee, W. Peng, and C. W. Kimball, *Physica C* **158**, 397 (1989).
13. P. A. Sterne and L. T. Wille, *Physica C* **162-164**, 225 (1988).
14. C. P. Burmester and L. T. Wille, *Phys. Rev.* **B40**, 8795 (1989).
15. G. Baumgartel and K. H. Bennemann, *Phys. Rev.* **B40**, 6711 (1989).
16. G. Baumgartel, P. J. Jensen, and K. H. Bennemann, *Phys. Rev.* **B42**, 288 (1990).
17. Z. X. Cai and S. D. Mahanti, *Phys. Rev.* **B40**, 6558 (1989).
18. T. Krekels, G. Van Tendeloo, D. Broddin, S. Amelinckx, L. Tanner, M. Mehbod, E. Vanlathem, and R. Deltour, to be published in *Physica C*.
19. H. J. Kistenmacher, *Phys. Rev.* **B38**, 8862 (1988).
20. S. Katsuyama, Y. Ueda, and K. Kosuge, *Physica C* **165**, 404 (1990).
21. J. L. Routbort, N. Chen, K. C. Goretta, and S. J. Rothman, Proceedings of ICMC 1990 Topical Conference: High Temperature Superconductors - Materials Aspects (in press).

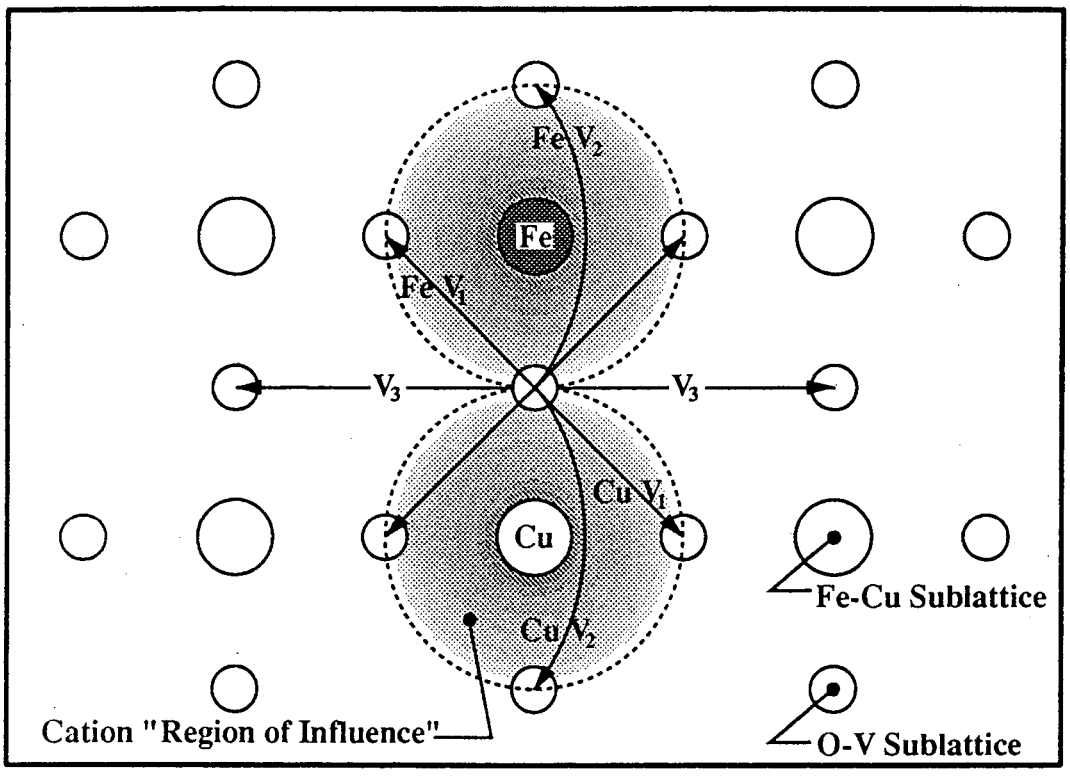

XBL 909-3045

Figure 1: Illustration of Iron and Copper influence on the oxygen-vacancy sublattice pair interactions for the model under investigation.

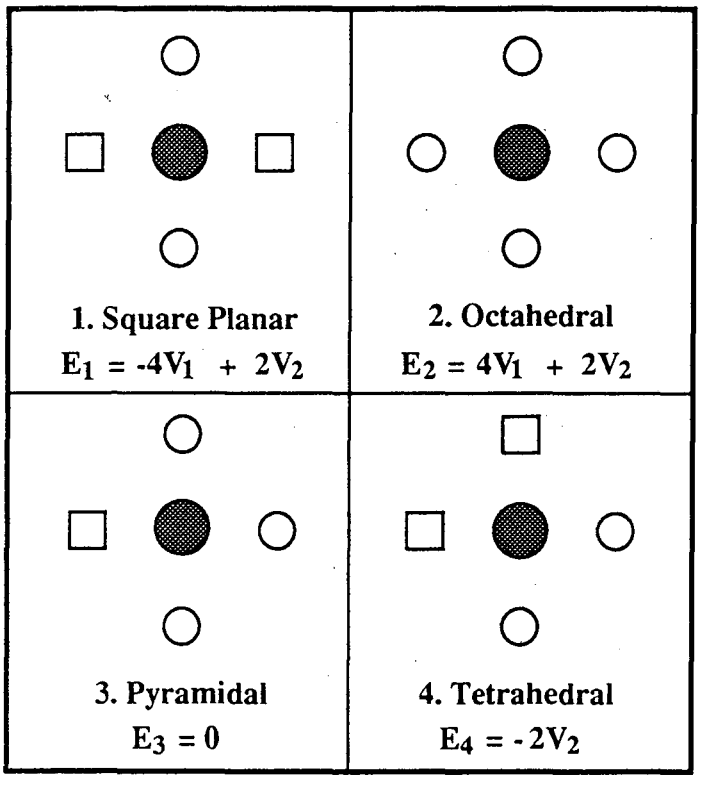

XBL 909-3046

Figure 2: Iron and nearest neighbor oxygen-vacancy clusters and associated energies used to derive bounding equations on the magnitude and sign of the V_1 and V_2 pair interactions for the current simulation.

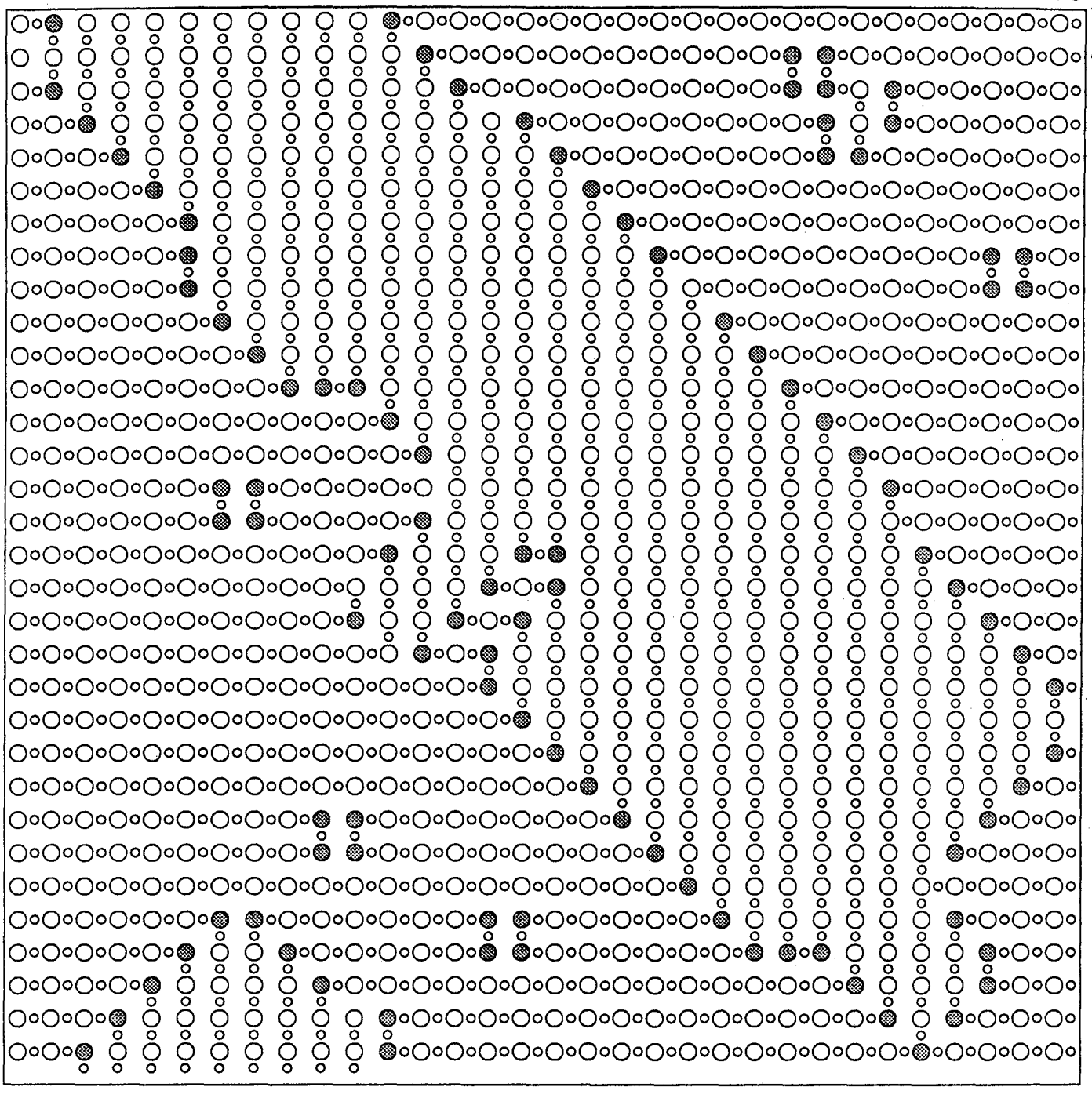

XBL 909-3047

Figure 3: Monte Carlo simulation snapshot of basal plane configuration obtained for 10 percent iron doping. Large filled circles represent irons, large unfilled circles coppers, and small circles oxygens. Notice how the irons form well ordered linear <11> clusters which percolate across the entire basal plane dividing the material into approximately equal proportions of orthogonal orthorhombic domains. Thus, while the local atomic arrangement is orthorhombic, the macroscopic symmetry of such a configuration is tetragonal. This snapshot was obtained by quenching the disordered structure from high temperature ($T = 10.0\ V_1/k_B$) and then annealing at constant temperature ($T = 0.8\ V_1/k_B$) and oxygen chemical potential ($\mu_O = 0.0$) for 100,000 Monte Carlo Steps/Site.

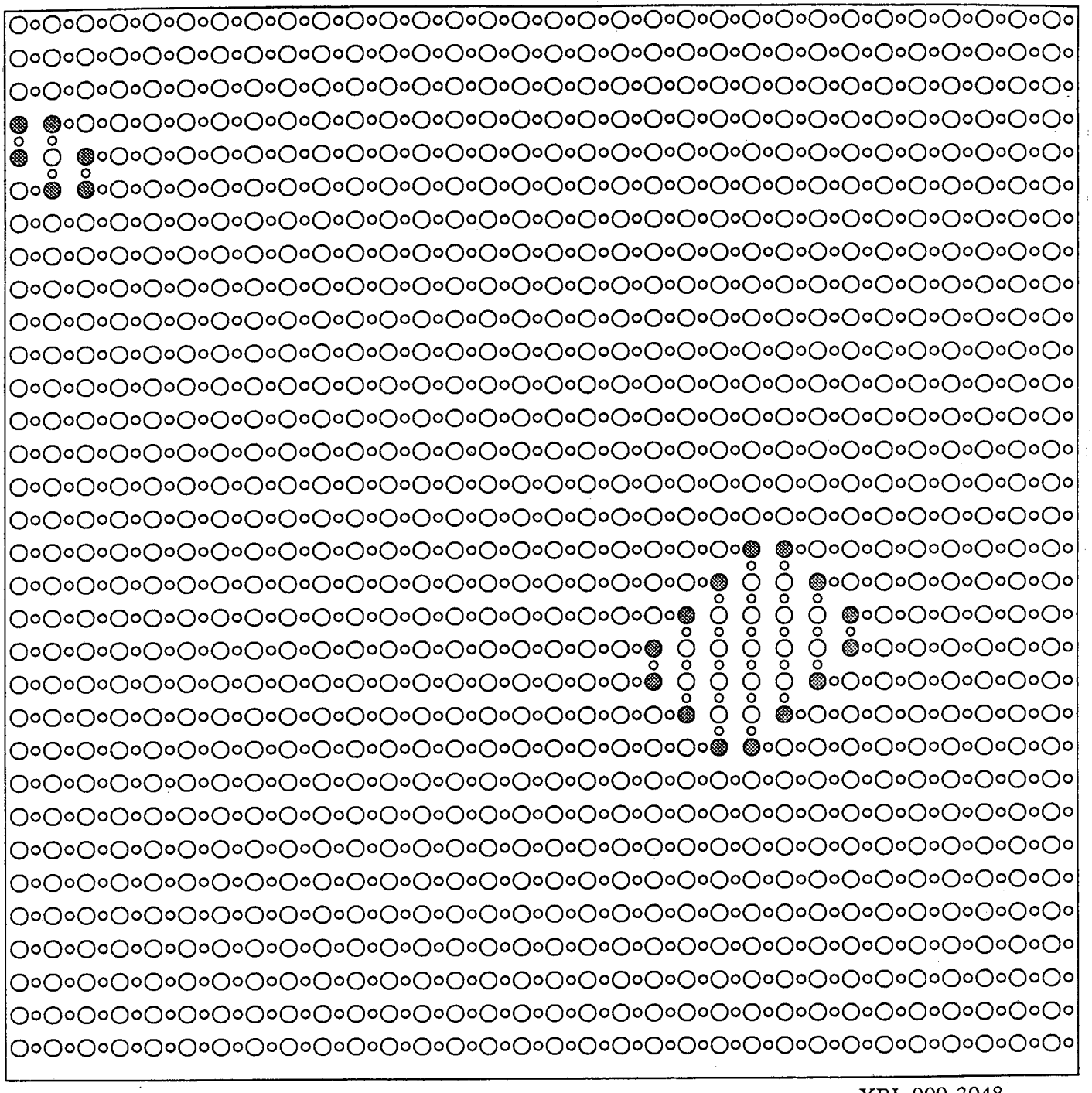

XBL 909-3048

Figure 4: Monte Carlo simulation snapshot of basal plane configuration for 2 percent iron doping. Notice how the irons form isolated subdomains within nearly single domain O-Cu-O chain structure leading to overall orthorhombic symmetry. This snapshot was obtained under the same simulation conditions detailed in Figure 3.

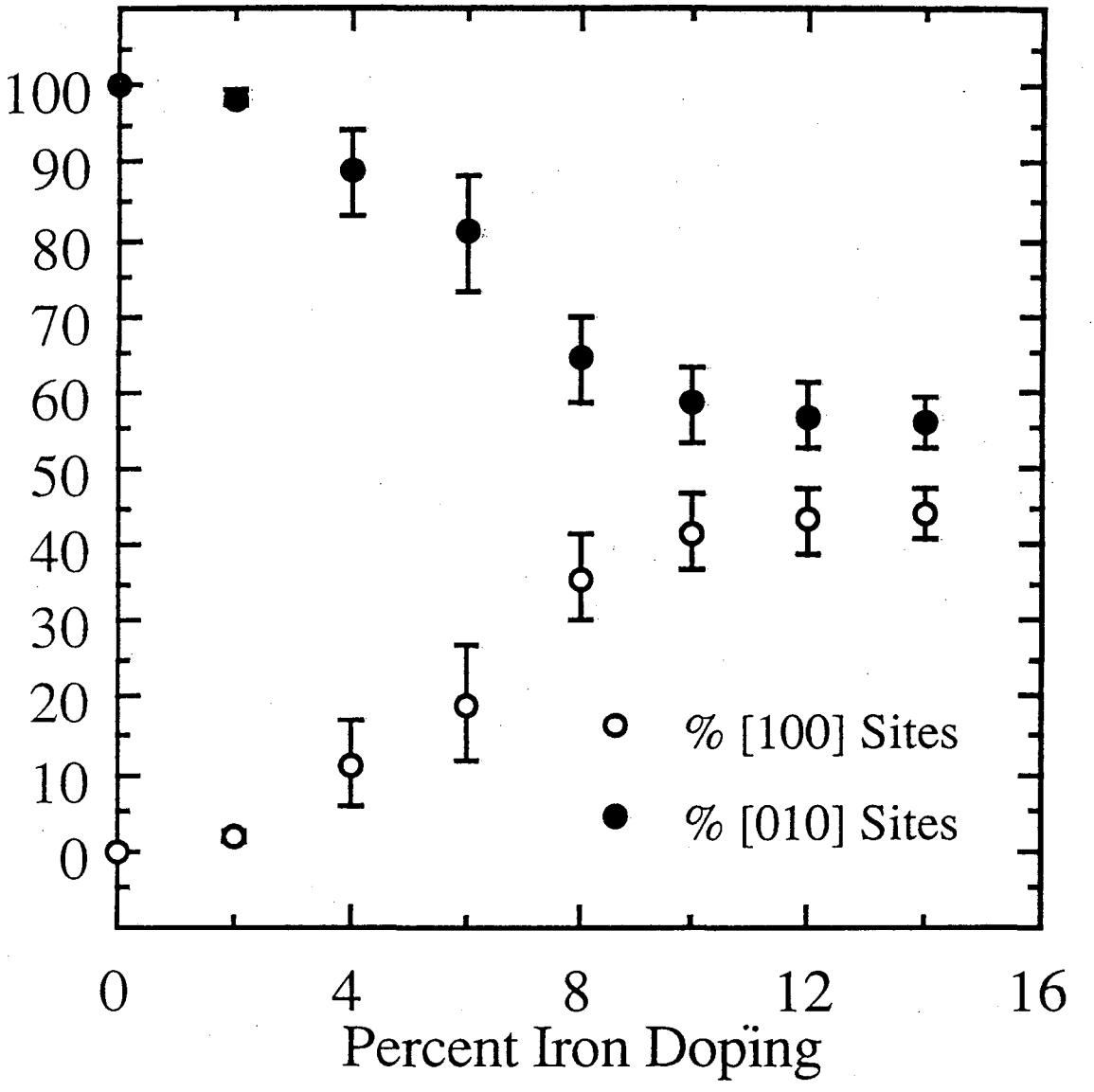

XBL 909-3049

Figure 5: Plot of the percentage of oxygen sites lying in either [100] or [010] orthorhombic domains vs. iron content in the basal plane of $YBa_2(Cu_{1-x}Fe_x)_3O_z$. Note the transition to macroscopic tetragonal symmetry occurring at approximately 8.5 percent basal plane iron content ($x \cong 0.028$). Error bars represent the standard deviation in the data from ten simulations for each point. Simulation conditions were identical to those used to obtain the configurations in Figures 3 and 4. Data presented here was obtained from a finite simulation lattice consisting of interpenetrating 32x32 Fe-Cu and 64x64 Oxygen-Vacancy sublattices.

LAWRENCE BERKELEY LABORATORY
UNIVERSITY OF CALIFORNIA
INFORMATION RESOURCES DEPARTMENT
BERKELEY, CALIFORNIA 94720